DEPARTMENT OF DEFENCE
DEFENCE SCIENCE & TECHNOLOGY ORGANISATION
DSTO

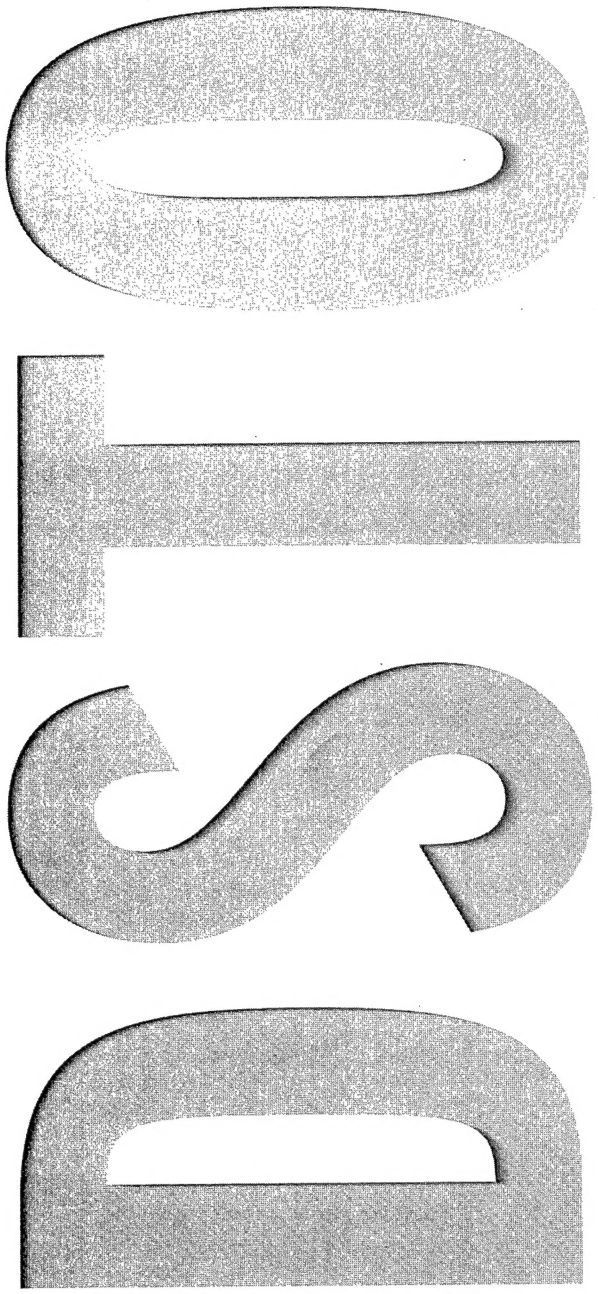

Analysis of Cyclic Mean Stress Relaxation and Strain Ratchetting Behaviour of Aluminium 7050

W. Hu, C.H. Wang and
S. Barter

DSTO-RR-0153

Analysis of Cyclic Mean Stress Relaxation and Strain Ratchetting Behaviour of Aluminium 7050

W. Hu, C.H. Wang and S. Barter

Airframes and Engines Division
Aeronautical and Maritime Research Laboratory

DSTO–RR–0153

ABSTRACT

The cyclic constitutive behaviour of aluminium 7050 under elstoplastic deformation has been investigated in this report. Experiments were performed under strain-controlled and stress-controlled cyclic loading, respectively, with a view to quantify the phenomena of mean stress relaxation and strain ratchetting. To mathematically describe the experimentally observed cyclic stress-strain behaviour, the framework of constitutive theory for rate-independent plasticity has been reviewed and the state-of-art development in the field summarised. A detailed discussion has been presented for a class of constitutive models which uses nonlinear differential equations to describe the kinematic hardening, using a single back stress or multiple back stresses.

Using the available steady-state experimental data, the material constants in the model have been identified. A comparison to the experimental results shows that the model can provide very good representation of the material stress–strain behaviour under cyclic loading, in terms of the general shape of hysteresis loops. A numerical procedure for determining the notch-root stress and strain from the applied remote stress or strain has also been developed. The significance of strain ratchetting on the prediction of fatigue crack initiation and growth life has also been discussed.

Further study is needed to improve the accuracy of prediction in the rate of stress relaxation.

DEPARTMENT OF DEFENCE

DEFENCE SCIENCE AND TECHNOLOGY ORGANISATION

Published by

DSTO Aeronautical and Maritime Research Laboratory
506 Lorimer St,
Fishermens Bend, Victoria, Australia 3207

Telephone: *(03) 9626 7000*
Facsimile: *(03) 9626 7999*

AR No. AR 010–989
June 1999

APPROVED FOR PUBLIC RELEASE

Analysis of Cyclic Mean Stress Relaxation and Strain Ratchetting Behaviour of Aluminium 7050

EXECUTIVE SUMMARY

In predicting fatigue life of components or structures, using either the local strain-based approach for crack initiation or the fracture mechanics-based approach for crack growth, an important input to the analysis is the material stress-strain response, or the constitutive relation, which predicts the current stress from a given strain history, at the point of interest. From a prescribed remote load history and a selected rule linking the remote load to the locate stress/strain at geometrical discontinuities such as a notch root, the constitutive model dictates the resulting hysteresis loops, and hence the corresponding damage incurred. It is, therefore, important that the constitutive relation adopted for a fatigue life model reflect the actual material behaviour as accurately as possible. This has been, however, restricted in the past by the demand on computing resources.

In this report, the transient cyclic stress-strain behaviour of aluminium 7050 has been studied experimentally and numerically. The results from strain- and stress-controlled tests demonstrated various phenomena such as the progressive relaxation of mean stress, the shakedown state when the mean stress approaches zero, the transient ratchetting, and the continuous ratchetting (plastic deformation) under certain cyclic stress loading. Within the framework of nonlinear kinematic hardening theory, a mathematical model has been developed and the material constants determined. The numerical results from the model correlate well with the experimental data when multiple back stresses are adopted. A numerical procedure has also been developed to determine the notch-root stress/strain from the given remote loading history, which can then be implemented in fatigue life prediction software such as `CI89`.

The results of this research now provide an improved capability in fatigue life assessment, especially for loading spectra dominated by overloads.

Authors

Weiping Hu
Airframes and Engine Division

Weiping Hu joined DSTO in 1998 as a research scientist, after working at several academic institutions including Dublin City University, Ireland, where he obtained his PhD degree in 1993; Monash University and Deakin University. His main research interests include metal plasticity and forming processes, numerical procedures for the finite element methods, continuum damage mechanics and the mathematical modelling of cyclic constitutive behaviour.

Chun Hui Wang
Airframes and Engine Division

Dr. Chun H. Wang joined DSTO in 1995 as a Senior Research Scientist. He is currently a Functional Head Damage Mechanics in the Airframes and Engines Division.

After completing his Ph.D in 1990 at the University of Sheffield, UK, he held various academic positions at the University of Sheffield, UK, the Univeristy of Sydney, and Deakin University. His research interests include fatigue and fracture mechanics, bonded joints and repairs, advanced composite materials, and constitutive modelling.

Simon Barter
Airframes and Engine Division

Simon Barter, Senior Professional Officer. Graduated from RMIT with a Diploma of Applied Science in Secondary Metallurgy (1982) and a Graduate Diploma in Surface Finishing and Corrosion Control (1987), both gained through part-time study while being employed at AMRL. He has been mostly involved with the metallurgical investigation of aircraft structures and components. These studies have included quantitative fractographic studies on Macchi, F111 and F/A-18 aircraft and research into fatigue crack growth in aircraft metals. His involvement in the investigation of numerous aircraft accidents has been the highlight of this work, having completed the Aircraft Accident Investigation course held at Cranfield Aviation Safety Centre. He now works in the Fatigue and Fracture Detection and Assessment area undertaking investigations into fatigue and fracture, aircraft accident investigation techniques and oxygen system materials compatibility.

Contents

NOMENCLATURE

$\boldsymbol{\sigma}$ Stress tensor

$\dot{\boldsymbol{\sigma}}$ Stress rate tensor

$\boldsymbol{\varepsilon}$ Strain tensor

$\boldsymbol{\varepsilon}^e$ Elastic strain tensor

$\boldsymbol{\varepsilon}^p$ Plastic strain tensor

$\dot{\boldsymbol{\varepsilon}}$ Strain rate tensor

$\dot{\boldsymbol{\varepsilon}}^p$ Plastic strain rate tensor

$\mathbf{S}$ Deviatoric stress tensor

$\mathbf{X}$ Back stress tensor

$\dot{\mathbf{X}}$ Back stress rate tensor

$\mathbf{N}$ Normal to the yield surface

$\mathbf{E}$ Elasticity tensor

f Yield surface

h Hardening modulus function

ϕ General yield function

J_2 von Mises yield function

ε^p Uniaxial plastic strain

R Isotropic hardening parameter

b, R_s Material constants for isotropic hardening

k_1, k_2 Material constants for kinematic hardening

p Equivalent plastic strain

$\dot{p}$ Equivalent plastic strain rate

$\dot{\lambda}$ Plastic multiplier

h Hardening modulus

ν A sign function depending on the direction of the plastic flow

Z Uniaxial back stress

σ Uniaxial stress

ε Uniaxial strain

$\Delta\sigma$ Uniaxial stress range

$\Delta\varepsilon$ Uniaxial strain range

$\Delta\varepsilon^p$ Plastic strain range

E Young's modulus

σ_0 Stress at the turning point

ε_0 Strain at the turning point

s Uniaxial remote stress

e Uniaxial remote strain

s_0 Uniaxial remote stress at the turning point

e_0 Uniaxial remote strain at the turning point

1 Introduction

For mechanical components subjected to asymmetric cyclic loading leading to plastic strain, most materials exhibit the phenomenon of either mean stress relaxation or strain ratchetting, or a combination of the two, depending on the applied load and structure geometry. If the maximum and minimum strains are fixed, then stress relaxation will occur. The initially non-zero mean stress will progressively shift towards zero as cyclic loading is applied, as sketched in Figure1a. This is analogous to stress relaxation under monotonic loading with fixed strain, except it is induced by the cyclic loading rather than the elapsed time. On the other hand, if the maximum and minimum stresses are controlled, then the so called strain ratchetting will take place, as shown schematically in Figure1b. Again, this is similar to creep under constant monotonic stress, but it is caused by the cyclic straining and the existence of a non-zero mean stress. Both strain ratchetting and mean stress relaxation are characterised by unclosed hysteresis loops, and plastic shakedown refers to the steady state reached after a certain number of cycles.

For a component with geometrical discontinuities, such as holes, cut-outs, notches and fillets, neither the stress nor the strain at the notch root is under control. Instead, the remote stress or strain is prescribed, while the local stress and strain are governed by the geometry of the discontinuity and the behaviour of the material. In this case both strain ratchetting and mean stress relaxation occur simultaneously. As ratchetting depends on the existence of a nonzero mean stress, it can be anticipated that the local mean stress will gradually relax, and that eventually the stress-strain loop will stabilize with a zero mean stress(Wang and Rose, 1998).

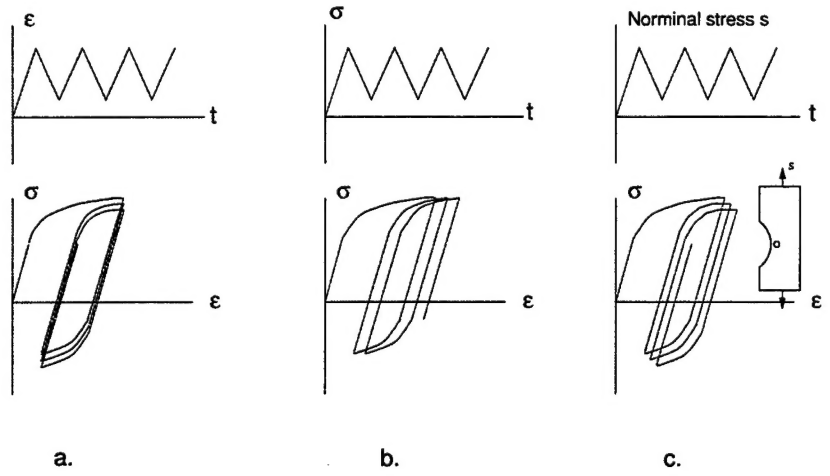

Figure 1: Elastoplastic deformation behaviour subjected to (a) constant cyclic strains (b) constant cyclic stresses and (c) remote constant nominal cyclic stresses.

Strain ratchetting could have a significant bearing on the prediction of structural integrity in terms of fatigue life and excessive plastic deformation. Figure 2 shows a block diagram of a fatigue prediction model using the local strain-based approach. Here, the strain–life curve is determined experimentally using smooth specimens, under fully-reversed straining. This curve serves as a look-up table, and if the fully-reversed strain range at a notch root can be determined (using Neuber (1961) rule, Glinka (1985) method, or an FE analysis) then the corresponding fatigue life can be

looked up from the curve. In practical problems, however, the remote stress amplitudes often vary from cycle to cycle and the cycles are not fully reversed, resulting in a nonzero mean stress. This remote mean stress leads to a nonzero local mean stress. The current engineering practice is to lump the effect of the nonzero mean stress into a factor and obtain an equivalent (fully-reversed) strain range which is then used to determine the corresponding fatigue life from the strain–life curve. The damage caused by such a cycle can then be accumulated by using a damage law such as Miner's linear rule. In determining the local stress and strain, the cyclic stress–strain behaviour is required, no matter which method is employed. While in practice materials may experience a considerable amount of transient cycling, especially in low cycle fatigue, the currently used cyclic stress-strain curves reflect only the steady-state response. Although this discrepancy is partially compensated by introducing a mean-stress factor, it introduces more uncertainty in the life prediction model.

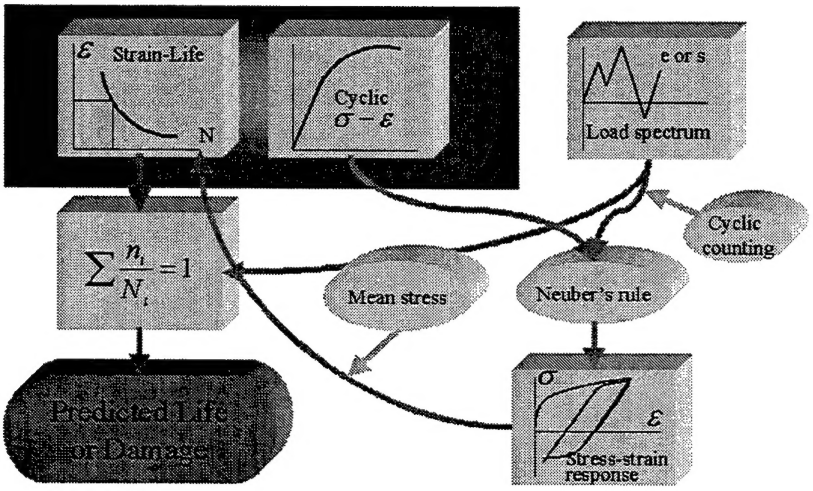

Figure 2: Block diagram for fatigue life prediction model

The transient stress–strain behaviour of the material described is not new (see Landgraf (1970), for example) but quite recently, research activities in this area have gained momentum probably because of (a) the rapid development in numerical techniques and computing hardware has made it possible to adopt more realistic constitutive models to improve life predictions, and (b) the ever increasing demand on reliability for high risk components such as aeronautical structures and nuclear facilities has made it necessary to search for more accurate material descriptions.

As a more general description of cyclic plasticity, a model for strain ratchetting should be capable of predicting the plastic strain in each branch of a cycle which leads to unclosed hysteresis loops, as well as the isotropic hardening and the general shape of the stress–strain loop. One of the difficulties in doing this is that the ratchetting strain is typically a small quantity in each cycle, and it may be transient or stable, depending on the type of material, temperature, the stress range and the magnitude of the mean stress.

From the viewpoint of metal physics, isotropic strain hardening can be interpreted as a result of the interaction of dislocations with precipitates, solid solution atoms, grains, cells, and subgrains, and can thus be approximately represented by a scalar hardening variable. In contrast, kinematic

hardening is a manifestation of existence of back stresses on the slip plane in the slip direction. It is thus orientation dependent and must be represented by a vector or tensor Stouffer and Dame (1996). The modelling of kinematic hardening can be traced back to the work of Prager (1949), in which the kinematic hardening is described by a back stress which is proportional to plastic strain. This model has gained wide acceptance and application especially in the analyses of metal forming, because of its simplicity, but it does not correctly describe the nonlinear dependence of stress on plastic strain. Refined models were subsequently developed by, among others, Besseling (1958), Armstrong and Frederick (1966), Mroz (1967), Krieg (1975), Dafalias and Popov (1976), and Cernosky and Krempl (1980). These models can be conveniently termed as classical, with the main attention directed at describing the cyclic behaviour, without emphasizing ratchetting. Indeed, most of the classical models are not suitable for predicting ratchetting, as investigated by Inoue et al. (1989) and Inoue et al. (1991).

Chaboche and Nouailhas (1989a) documented experimental evidence of ratchetting under uniaxial and multiaxial loading conditions. In terms of the magnitude of mean stress relative to stress range, two types of loading conditions are distinguished: quasi-reversed, for which the mean stress is very small comparable to the stress range, and quasi-repeated, for which the mean stress is compared to the stress range. Based on experiments performed on various materials, several conclusions have been drawn for the quasi-reversed loading, assuming there exists a nonzero mean stress and nonzero inelastic strain range:

- there is always some transient ratchetting;
- shakedown may take place after a certain number of cycles;
- the transient ratchetting increases when the mean stress is increased, keeping the stress range constant;
- for sufficiently high mean stress, shakedown could be replaced by a continuous ratchetting, with its rate dependent on the magnitude of the mean stress;
- the transient ratchetting increases when the stress range is increased.

Chaboche and Nouailhas (1989b) investigated the modeling possibilities of several linear and nonlinear-kinematic hardening rules in the frame work of time-independent plasticity. All the models are based on three or four back stresses, with the first two obeying the nonlinear-kinematic rule, and the third one obeying either linear- or nonlinear-kinematic rule. A fourth back stress, obeying either a generalized Prager rule or a rule proposed by Rousselier et al. (1985), could optionally be introduced. It has been demonstrated by Chaboche and Nouailhas (1989b) that the model proposed by Rousselier offers the best compromise.

Jiang and Sehitoglu (1996a,b) investigated ratchetting occurring in steel 1070 for railroad applications. It has been observed that it is not always true that ratchetting occurs in the direction of nonzero mean stress, even for proportional loading. A threshold term has been introduced to an Armstrong-Frederick type constitutive model.

Motivated by the requirement to accurately compute the plastic energy dissipation in a load cycle, Xia and Ellyin (1991) studied ratchetting under out-of-phase cyclic loading for low alloy carbon steel. An extra hardening phenomenon has been observed in addition to the anisotropy due to the plastic deformation. Xia and Ellyin (1994) studied the biaxial ratchetting under strain

or stress-controlled axial cycling with constant hoop stress using thin-walled tubular specimens of 304 stainless steel. In axial strain-controlled mode ratchetting was observed in the hoop direction, and under stress-controlled mode ratchetting was observed in both the hoop and the axial direction. A two surface modelDafalias and Popov (1976) has been used to simulate the results, but different evolution rules have been adopted for the monotonic loading and the plastic reloading mode.

Within the rate-independent framework, there are basically two approaches in attempting to describe the cyclic stress–strain behaviour. In the first (Mroz, 1967), the essentially curvilinear stress–strain relation is linearized, just like in uniaxial loading the stress-strain curve can be represented approximately using a number of straight line segments. The linearization results in a series of yield surfaces, each with its own centre and size. The direction of plastic flow is still governed by the normal to the current yield surface. The yield surfaces cannot intersect, but they can consecutively act in contact and move together. The direction of the movement of the current yield surface is such that at the point of contact the current (and others inside it) and the subsequent yield surface have the same normal. This model can correctly describe the nonlinearity of the stress–strain loops, particularly under cyclically stable conditions, and the cyclic hardening or softening of the material with asymptotic plastic shakedown. It does not, however, predict ratchetting at all.

Dafalias and Popov (1976) proposed a similar model but with only two surfaces, with one acting as a yield surface and the other a limiting surface analogous to the subsequent yield surface in the Mroz model. The translation rule for the yield surface, which characterizes the kinematic hardening, can be specified independently, while that for the limiting surface is determined by the requirement that the two surfaces must have the same outward normal at contact. By contrast to the Mroz model, this model requires only two surfaces, and is thus much simpler to identify and more economic to implement in numerical procedures. The continuously varying plastic modulus employed would allow the description of a smooth elastic-plastic transition. A similar two surface model has been studied by Krieg (1975).

The second class of constitutive models for rate-independent cyclic plasticity is characterized by the explicit specification of a translation rule for the back stress through differential equations. The classical Prager (1949) model, for instance, can be expressed as $\dot{\mathbf{X}} = k_1 \dot{\boldsymbol{\varepsilon}}$, giving a linear relation between the back stress $\mathbf{X}$ and the plastic strain $\boldsymbol{\varepsilon}^p$. By employing appropriate differential equations for the back stress, it is possible to predict the nonlinear behaviour of the cyclic stress-strain loop and strain ratchetting, as demonstrated by the Armstrong-Frederick (Armstrong and Frederick, 1966) model. The advantages of this model are that each back stress can be described by just two material constants and these constants can be determined from the stable cyclic stress–strain curve. In the following the A-F theory is first outlined, and it is then studied in more detail for the modelling of ratchetting of aluminium 7050.

In this report, the strain ratchetting/mean stress relaxation phenomena are documented for aluminium 7050. Strain- and stress-controlled experiments have been conducted under tension-compression loading using specimens with uniform gauge sections. The framework of constitutive theories for cyclic plasticity is reviewed, and an Armstrong-Frederick type model is used to model the experimental observations.

2 Experimental Results

The material being considered was aluminium 7050-T7451 which is used for the aft fuselage stub frames on F/A-18 fighter planes. It has a nominal yield stress of $\sigma_y = 483$ MPa (70 ksi) and Young's modulus of $E = 69$ GPa (10,000 ksi). The specimens used for the tests are of cylindrical shape with a uniform gauge section having a diameter of 12 mm, as shown in 3. A dynamic clip gauge, with a gauge length of 12.5 mm and a capacity of ± 2.5 mm, was used to measure and control the axial strain. The experiments were conducted at room temperature on a 100 kN

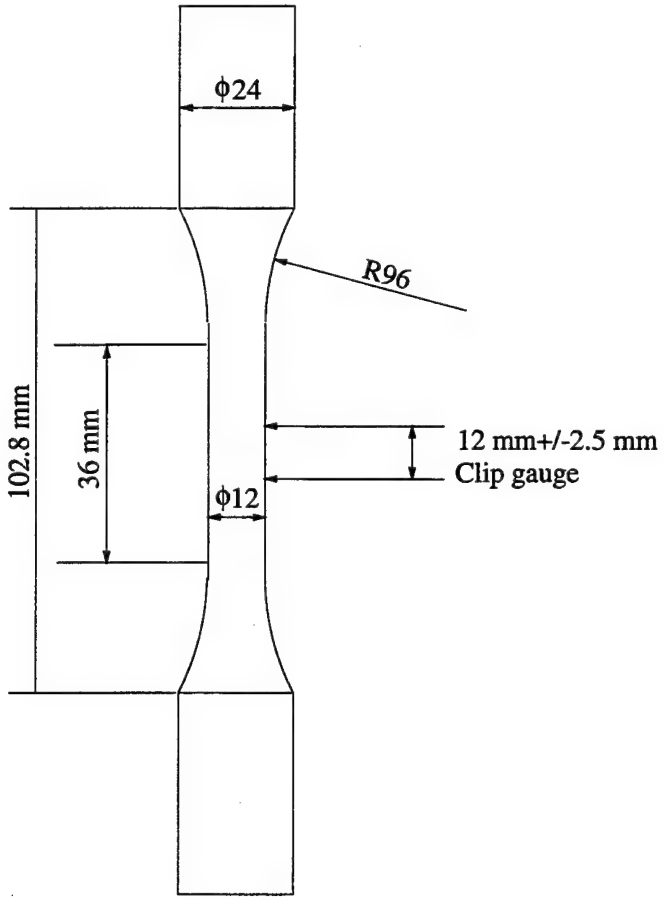

Figure 3: Specimen details

Instron 810 Material Test System and the nominal loading conditions for strain- and stress-control are listed in Table 1. The actual values attained were slightly different from these because of the limitation of the servo-control mechanism.

Table 1: Loading conditions for stress- and strain-controlled tests

Test ID	Specimen ID	Strain–control		Stress–control (MPa)	
		Min	Max	Min	Max
1	kp1e3	0.002	0.02		
2	kp1d3pt3			-327	462
3	kp1d13	0.002	0.02		
		0.006	0.02		
		0.008	0.02		
		0.010	0.02		
		0.002	0.02		

2.1 Mean stress relaxation

Figure 4 shows the results of Test 1, demonstrating the relaxation of mean stress and the eventual plastic shakedown, under strain-controlled loading with an initial positive mean stress. It can be immediately seen that the hysteresis loops shift downwards as cycling progresses, and stabilizes after a certain number of cycles (in this case, about 200). At the steady state, the stress cycles become symmetric, with an amplitude of $\sigma_a = 437$ MPa. A closer examination of the loops reveals that although each hysteresis loop shifts downward as a whole, the amount of shift differs at different strain points. In particular, the stress at the lower strain limit decreases faster than that at the upper strain limit. In effect, this means that for the prescribed strain range the stress range increases, or the material (isotropically) strain-hardens. Figure 5 plots the relation between the half strain range and the number of cycles, which indicates that the isotropic hardening reaches saturation after about 60 cycles, or an equivalent plastic strain of about 0.72, as each half cycle incurs a plastic strain of approximately 0.0059.

Figure 6 demonstrates the reduction of mean stress as the cycling progresses. It is apparent that the mean stress reduction is rapid in the first few cycles, but the rate of shakedown decays rapidly. After 60 cycles, the mean stress reaches 3 MPa, but it takes another hundred or so cycles before it reaches zero.

2.2 Strain ratchetting

Figure 7 shows the results from the stress-controlled test, Test 2, which demonstrate the progressive straining of the specimen as cycling progresses. The asymmetric stress cycle (−327—463) can be viewed as a fully–reversed cycle (the primary load) superposed on a constant mean stress (the secondary load), and the amount of strain ratchetting in a cycle is determined by the magnitude of the mean stress and the range of plastic strain. Geometrically, the forward and backward branch of the hysteresis loop are different due to different amount of plastic straining.

As the underlying mechanism is the same for mean stress relaxation and strain ratchetting, subsequent discussions will be focused on the former, but the formulation is readily applicable to the latter.

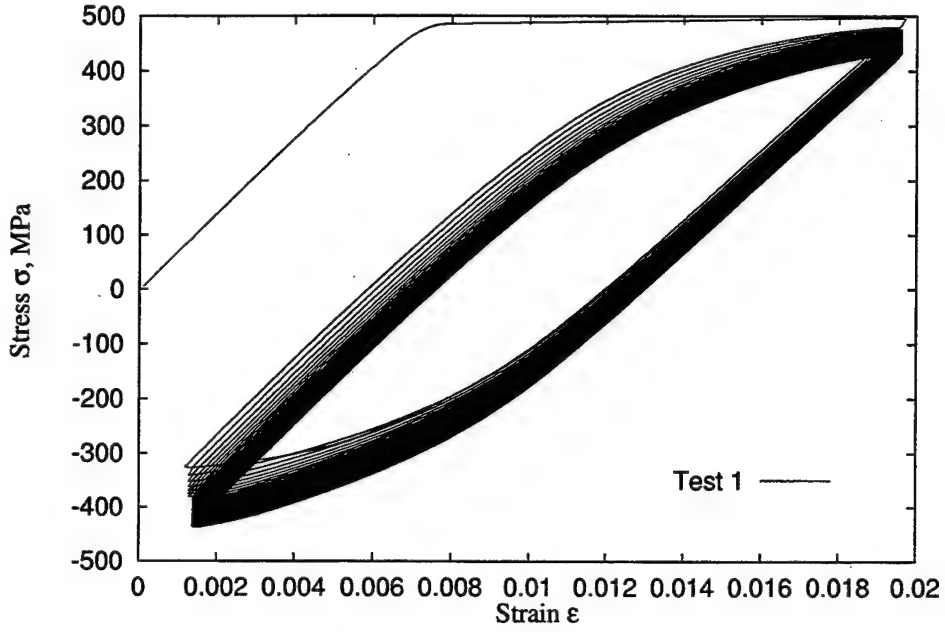

Figure 4: Experimental results for mean stress relaxation under strain–controlled cyclic loading

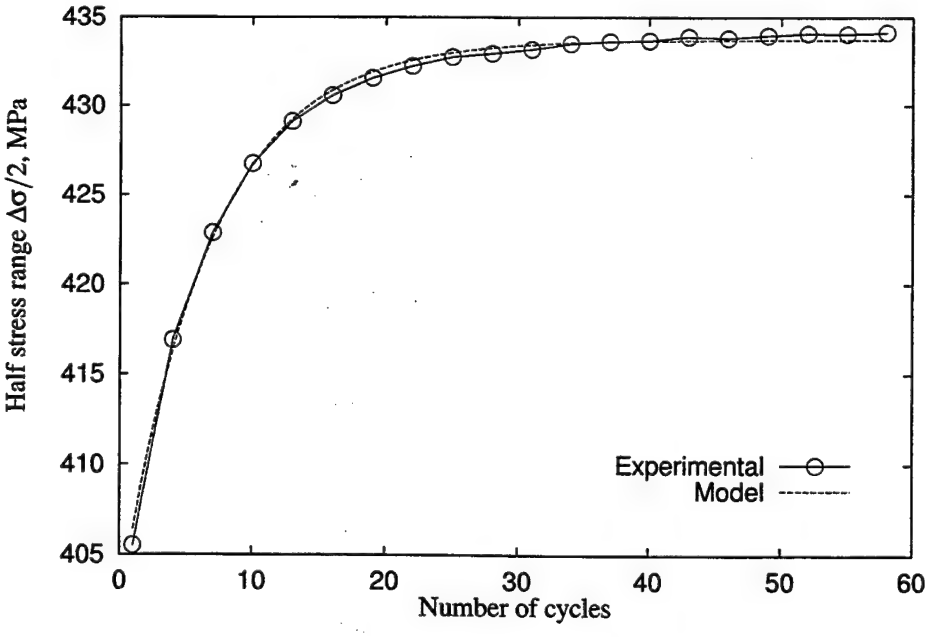

Figure 5: Isotropic hardening curve

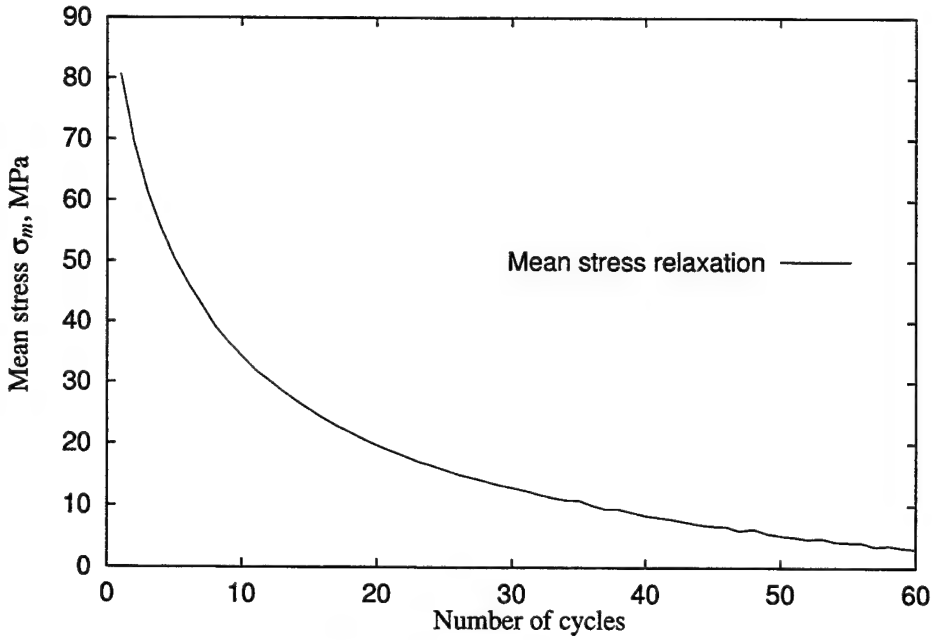

Figure 6: Mean stress relaxation

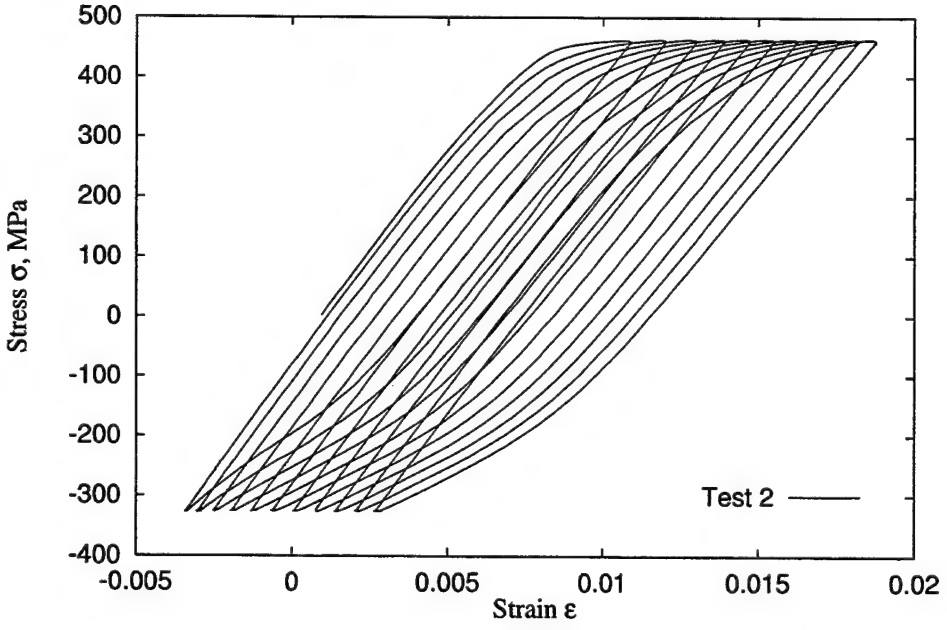

Figure 7: Experimental results for strain ratchetting under stress control.

2.3 Effect of strain range on ratchetting

In Test 3 (see Table 1) similar loading condition as that in Test 1 was applied, except that the strain range was varied by increasing the lower strain limit from 0.002 to 0.01 while keeping the upper limit fixed at 0.02. The detailed loading schedule is as follows,

- Step 1: 150 cycles at a strain range of 0.002∼0.02
- Step 2: 100 cycles at a strain range of 0.006∼0.02
- Step 3: 100 cycles at a strain range of 0.008∼0.02
- Step 4: 100 cycles at a strain range of 0.010∼0.02
- Step 5: cycling until failure at a strain range of 0.002∼0.02.

Figure 8(a)–8(d) present the cyclic responses from these tests. Clearly, mean stress relaxation occurs only when there is plastic deformation in a cycle, and the range of the plastic strain dictates the rate of relaxation. In Figure 8(a) the plastic strain range is 0.018 and full relaxation is achieved in about 150 cycles, while Figure 8(d) shows hardly any relaxation as the cycles are essentially elastic. Figure 9 illustrates the hysteresis loops at load Step 5, which is the same as Step 1. It should be noted that the hysteresis loops did not immediately reach the steady state, although the material has already undergone a few hundreds of cycles at various strain levels. This is due to the negative mean stress induced when the applied load changes to a higher magnitude.

Figure 10 shows a comparison of mean stress relaxation for Test 1 and different loading steps in Test 3. Clearly, full relaxation of mean stress can only be achieved if there exists sufficient plastic strain in each cycle. For cycles with negligible plastic strain, the mean stress essentially remains unchanged, as indicated by the results of Test 3, Step 3 and 4. It is interesting to note the slightly negative mean stress for load Step 5, which then relaxes to zero.

Figure 11 presents the cyclic isotropic hardening characteristics. It should be noted that since Test 3 Step 5 was performed after all the cycles in Step 1, it can be viewed as a continuation of the hardening curve for Step 1. Obviously the isotropic hardening has essentially saturated after 60 cycles in Step 1.

3 Framework of Constitutive Models

In the following, the discussion is limited to time-independent structure of constitutive theories, which are appropriate for modelling the deformation behaviour of most metallic structural alloys at room temperature. In this case, small-strain plasticity theory assumes that the total strain, $\boldsymbol{\varepsilon}$, can be decomposed into an elastic part $\boldsymbol{\varepsilon}^e$ and a plastic part $\boldsymbol{\varepsilon}^p$,

$$\boldsymbol{\varepsilon} = \boldsymbol{\varepsilon}^e + \boldsymbol{\varepsilon}^p, \tag{1}$$

and the stress is related to the elastic strain through the generalized Hooke's law,

$$\boldsymbol{\sigma} = \mathbf{E} : (\boldsymbol{\varepsilon} - \boldsymbol{\varepsilon}^p). \tag{2}$$

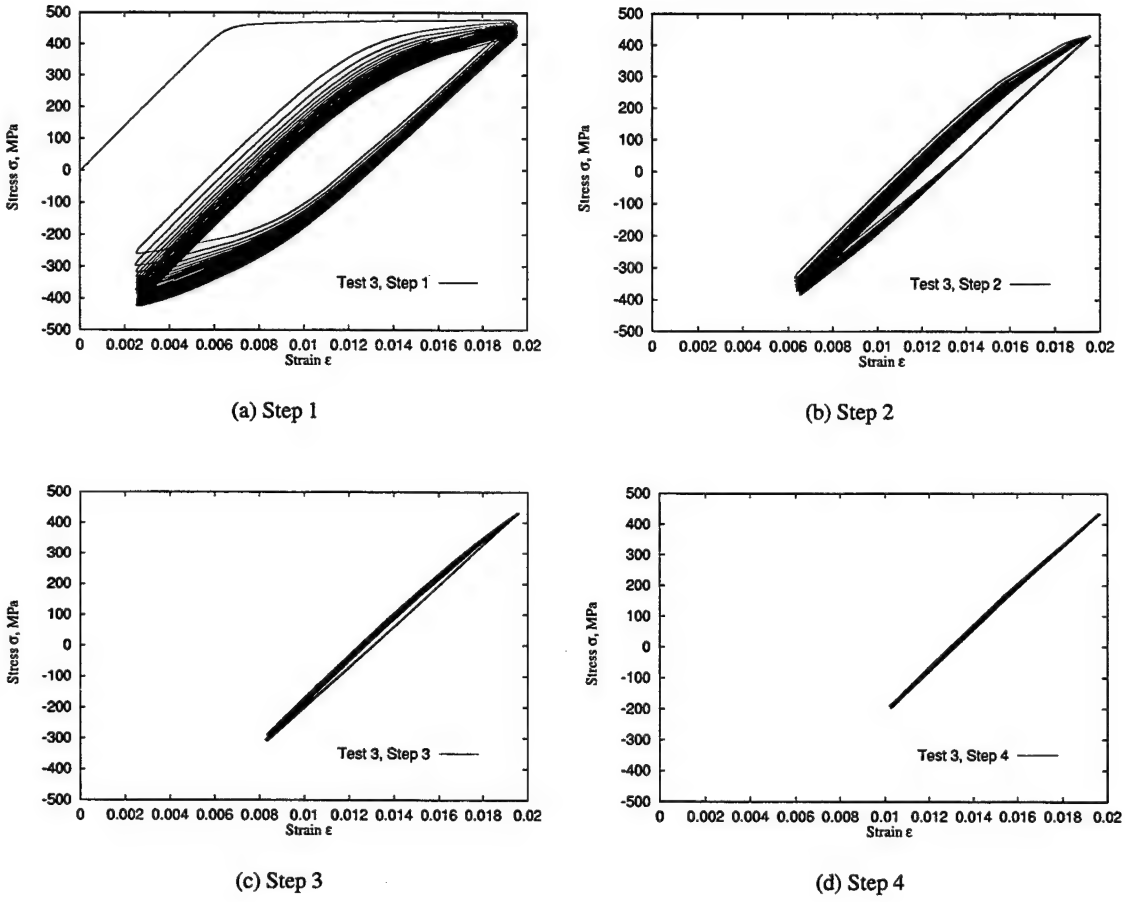

(a) Step 1

(b) Step 2

(c) Step 3

(d) Step 4

Figure 8: Comparison of mean stress relaxation under different strain range

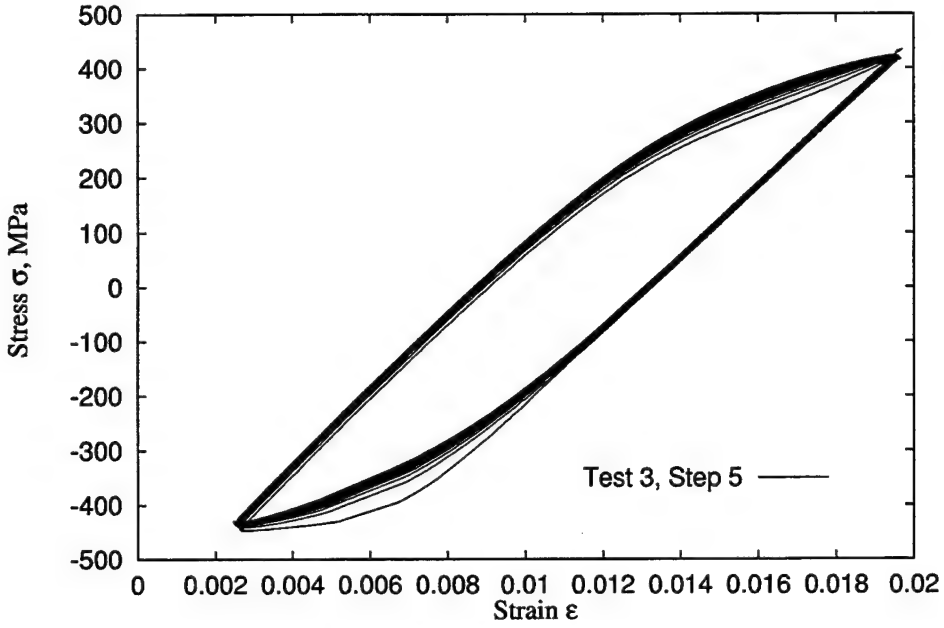

Figure 9: Hysteresis loops at load step 5, Test 3.

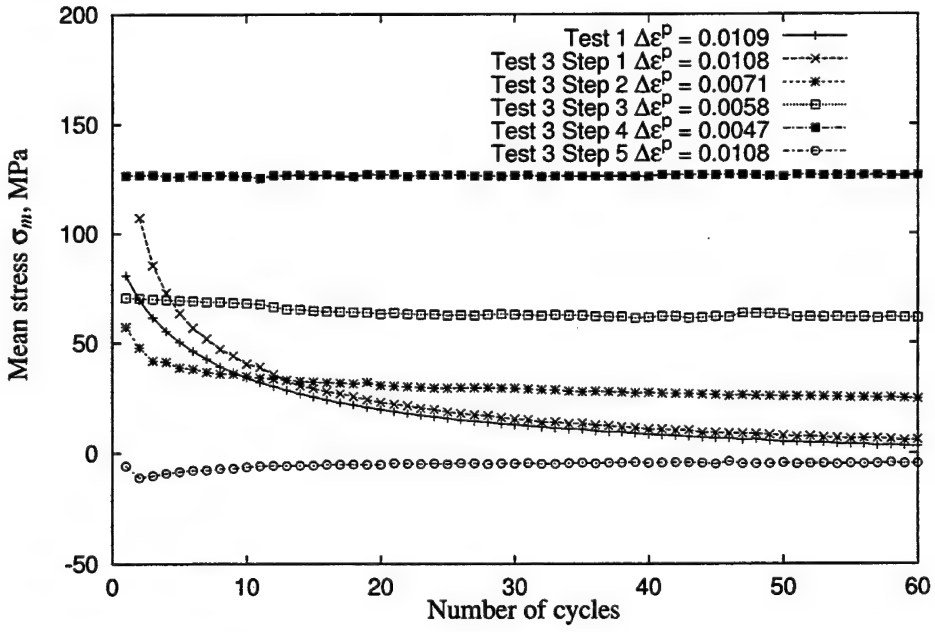

Figure 10: Comparison of mean stress relaxation under different strain ranges

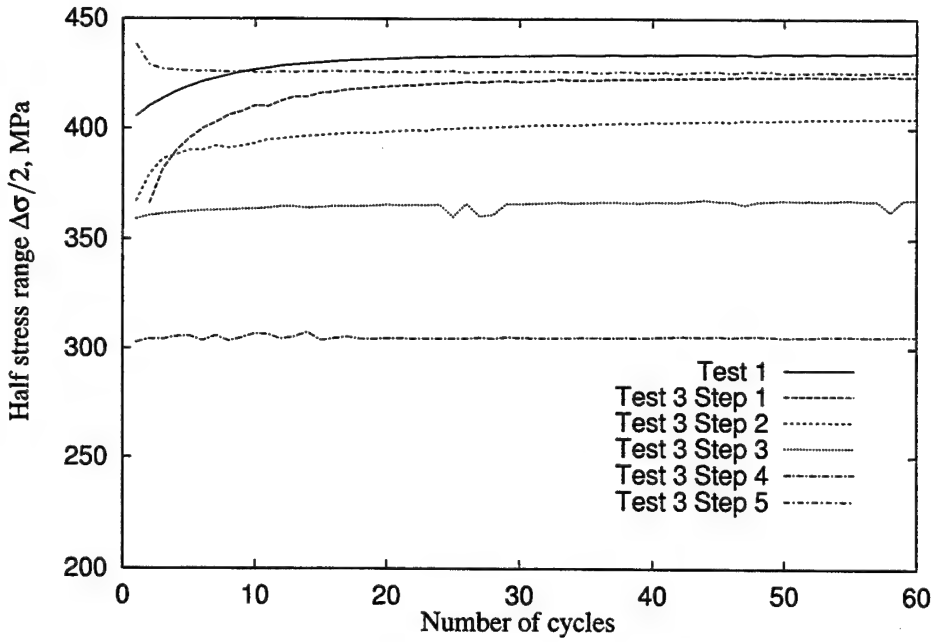

Figure 11: Comparison of cyclic strain hardening for different strain range

Here, the bold symbols represent tensorial quantities, and ":" signifies the scalar product, $\boldsymbol{x} : \boldsymbol{y} = x_{ij} y_{ij}$ (repeated indices imply summation). $\mathbf{E}$ is the fourth-order tensor of elasticity.

Let σ_y be the uniaxial yield stress, and R an internal variable describing isotropic hardening, then a yield surface can generally be described by

$$f = \phi(\boldsymbol{\sigma} - \mathbf{X}) - R - \sigma_y = 0. \tag{3}$$

Here, the isotropic hardening parameter R can be expressed as a function of the equivalent plastic strain p, *i.e.*

$$R = R(p),$$

with p defined through

$$\dot{p} = \left[\frac{2}{3} \dot{\boldsymbol{\varepsilon}}^p : \dot{\boldsymbol{\varepsilon}}^p \right]^{1/2}. \tag{4}$$

In the above, and henceforth, the superposed dot "." signifies the differentiation with respect to a time-like variable, as the real time is irrelevant for rate-independent materials.

In Eq. (3) $\mathbf{X}$ is known as the back stress tensor, and it plays the key role in the modelling of the kinematic hardening behaviour of the material. Indeed, the earlier work on kinematic hardening by Prager (1949) is given by

$$\mathbf{X} = k_1 \boldsymbol{\varepsilon}^p \tag{5}$$

This simple model has been widely used to describe the Bauchinger effect observed in experiments, and for solving metal forming problems, but because of the linear relation between $\mathbf{X}$

and $\boldsymbol{\varepsilon}^p$, it cannot qualitatively reflect the curvilinear nature of kinematic hardening as sketched in Figure 1.

For Armstrong-Frederick type of models, the evolution rule for $\mathbf{X}$ can be given explicitly as

$$\dot{\mathbf{X}} = \frac{2}{3}k_1\dot{\boldsymbol{\varepsilon}}^p - k_2\mathbf{X}\dot{p} \tag{6}$$

where k_1 and k_2 are material constants.

The direction of the plastic flow is determined by the normality rule, *i.e.*,

$$\dot{\boldsymbol{\varepsilon}}^p = \mathbf{N}\dot{\lambda} \tag{7}$$

where $\mathbf{N} = \partial f/\partial\boldsymbol{\sigma}$ is the normal to the yield surface.

Using Eq. (4) and (7) we obtain the relation between the equivalent plastic strain rate $\dot{p}$ and the plastic multiplier $\dot{\lambda}$

$$\dot{p} = \left(\frac{2}{3}\dot{\boldsymbol{\varepsilon}}^p : \dot{\boldsymbol{\varepsilon}}^p\right)^{1/2} = \left(\frac{2}{3}\mathbf{N} : \mathbf{N}\right)^{1/2}\dot{\lambda}. \tag{8}$$

where $\dot{\lambda}$ is to be determined using the consistency condition $\dot{f} = 0$.

In addition, the following relations hold true

$$\dot{p} \geq 0, \quad \dot{p}f = 0 \text{ and } \dot{p}\dot{f} = 0 \tag{9}$$

for plastic deformation.

The plastic multiplier $\dot{\lambda}$ in Eq. 7 can now be determined by applying the consistency condition, *i.e.*, that the stress state must lie on the yield surface,

$$\dot{f} = 0 = \frac{\partial f}{\partial\boldsymbol{\sigma}} : \dot{\boldsymbol{\sigma}} + \frac{\partial f}{\partial\mathbf{X}} : \dot{\mathbf{X}} + \frac{\partial R}{\partial p}\dot{p} \tag{10}$$

Noting that $\partial f/\partial\boldsymbol{\sigma} = -\partial f/\partial\mathbf{X}$, and denoting $\partial R/\partial p = R'$, we get

$$\dot{\lambda} = < \frac{1}{h}\mathbf{N} : \dot{\boldsymbol{\sigma}} > \tag{11}$$

where "$< . >$" denotes the MacCauley bracket, i.e.,

$$< u > = \frac{1}{2}(u + |u|)$$

and the hardening modulus h is given by

$$h = k_1\mathbf{N} : \mathbf{N} - (k_2\mathbf{X} : \mathbf{N} - R')\left(\frac{2}{3}\mathbf{N} : \mathbf{N}\right)^{1/2} \tag{12}$$

3.1 J_2 theory

The derivations presented above is applicable to a general yield function ϕ. In the case of the von Mises yield criterion, $\phi = J_2$, the above expressions can be simplified. First we note that the back stress as defined in Eq. 6 is a deviatoric tensor if plastic incompressibility applies. This is evident by considering the trace of $\mathbf{X}$ in the equation. As a deviatoric tensor, we may use $\mathbf{X}$ to denote the back stress as well as its deviatoric tensor. Thus, if the deviatoric stress tensor is given by $\mathbf{S}$, we have

$$\phi = J_2(\boldsymbol{\sigma} - \mathbf{X}) = \left[\frac{3}{2}(\mathbf{S} - \mathbf{X}) : (\mathbf{S} - \mathbf{X})\right]^{\frac{1}{2}} \tag{13}$$

as the yield function, and the differentiation with respect to $\boldsymbol{\sigma}$ gives

$$\mathbf{N} = \frac{\partial f}{\partial \boldsymbol{\sigma}} = \frac{\partial J_2}{\partial \boldsymbol{\sigma}} = \frac{3}{2}\frac{\mathbf{S} - \mathbf{X}}{J_2} \tag{14}$$

Using this expression for $\mathbf{N}$, we get

$$\mathbf{N} : \mathbf{N} = \frac{3}{2} \tag{15}$$

Thus, Eq. (8) and (12) can be simplified, respectively, to

$$\dot{p} = \dot{\lambda},$$

and

$$h = k_1 - k_2 \mathbf{X} : \mathbf{N} + R'.$$

In the following, only J_2 theory will be considered.

3.2 Isotropic hardening rules

In the above discussion, the isotropic hardening has been assumed to be a function of the equivalent plastic strain, but the explicit form of $R = R(p)$ has not been specified. As an independent hardening mechanism, the isotropic hardening rule can be selected without reference to the kinematic hardening rule. For isothermal plastic deformation, Chaboche (1986) suggested that the following form can be used

$$\mathrm{d}R = b(R_s - R)\mathrm{d}p, \tag{16}$$

where R_s and b are two material constants. This equation states that irrespective of the kinematic rule and the loading condition (symmetric or unsymmetric), the internal stress R varies as a function of the accumulated equivalent plastic strain p. Using experimental data for steel 316, Chaboche (1986) has shown that the the ratio of R/R_s can indeed be expressed as a function of p only.

3.3 Model Identification

In order to determine the material constants in the model from experimental data, the model description given above can be recast into the form for uniaxial loading where $\sigma_{ij} = 0$ except $\sigma = \sigma_{11} \neq 0$. Adopting the assumption of plastic incompressibility, we have $\dot{\varepsilon}^p = \dot{\varepsilon}^p_{11} \neq 0, \dot{\varepsilon}^p_{22} = \dot{\varepsilon}^p_{33} = -\frac{1}{2}\dot{\varepsilon}^p$ which gives the equivalent plastic strain rate as $\dot{p} = \sqrt{\frac{2}{3}\dot{\boldsymbol{\varepsilon}}^p : \dot{\boldsymbol{\varepsilon}}^p} = |\dot{\varepsilon}^p|$. Further, as the back stress $\mathbf{X}$ is a deviatoric tensor, we have $X_{11} = X$ and $X_{22} = X_{33} = -\frac{1}{2}X$. And similarly, $S_{11} = \frac{2}{3}\sigma, S_{22} = S_{33} = -\frac{1}{3}\sigma$. Using these expressions in Eq. (3), the yield surface is given by $f = |\sigma - \frac{3}{2}X|$. By taking $\frac{3}{2}X$ as the new back stress but still denoting it as Z, we get the following set of equations for the model in uniaxial loading,

$$f = |\sigma - Z| - R(p) - \sigma_y = 0 \tag{17}$$

$$\dot{p} = \frac{1}{h} < \nu\dot{\sigma} > \tag{18}$$

$$h = \frac{3}{2}k_1 - \nu k_2 Z \tag{19}$$

$$\dot{Z} = k_1\dot{\varepsilon}^p - k_2 Z|\dot{\varepsilon}^p| \tag{20}$$

where $\nu = \text{sign}(\dot{\sigma}) = \pm 1$, depending on the direction of the plastic flow. Let the initial values for plastic strain and the back stress be ε^p_0 and X_0 at the beginning of each half cycle, then the above uniaxial model can be integrated to give

$$Z(\varepsilon^p) = \nu\frac{k_1}{k_2} + \left(Z_0 - \nu\frac{k_1}{k_2}\right) e^{-\nu k_2(\varepsilon^p - \varepsilon^p_0)}, \tag{21}$$

where k_1 and k_2 are two material constants to be determined experimentally. Obviously, the non-linear dependency of back stress on plastic strain is introduced by the second term, which decays as the relative plastic strain $\varepsilon^p - \varepsilon^p_0$ increases. For sufficiently large $\varepsilon^p - \varepsilon^p_0$, Z saturates to $\nu k_1/k_2$.

Once the back stress in known, the corresponding stress can be determined from the yield criterion

$$\sigma = Z + \nu(R + \sigma_y) \tag{22}$$

It should be mentioned that the above model applies to stabilized cycles as well as transient ones. In a stable cycle, the isotropic variable reaches its maximum value of R_s, and the maximum and minimum values $(\sigma_{max}, \varepsilon_{max})$ and $(\sigma_{min}, \varepsilon_{min})$ are all constant during a cycle. Furthermore, the plastic strain at the end of one excursion (the loading branch, say) will be the initial value of the next one (the unloading and reloading branch). From Eq. (21) the maximum and minimum back stress can then be expressed as

$$Z_{max} = \frac{k_1}{k_2} + \left(Z_{min} - \frac{k_1}{k_2}\right) e^{-k_2(\varepsilon^p_{max} - \varepsilon^p_{min})} \tag{23}$$

$$Z_{min} = -\frac{k_1}{k_2} + \left(Z_{max} + \frac{k_1}{k_2}\right) e^{k_2(\varepsilon^p_{min} - \varepsilon^p_{max})} \tag{24}$$

Denoting the plastic strain range as $\Delta\varepsilon^p = \varepsilon^p_{max} - \varepsilon^p_{min}$, the stress range as $\Delta\sigma = \sigma_{max} - \sigma_{min}$, and using the fact that

$$\sigma_{max} = Z_{max} + R_s + \sigma_y, \tag{25}$$

$$\sigma_{min} = Z_{min} - R_s - \sigma_y, \tag{26}$$

Eq. (23) and (24) can be solved to give the relation between the half stress range and half strain range under stabilized cycling,

$$\frac{\Delta\sigma}{2} = \frac{k_1}{k_2}\tanh(k_2\frac{\Delta\varepsilon^p}{2}) + \sigma_y + R_s. \tag{27}$$

The significance of the above equation is that it provides a means for determining the material constants k_1 and k_2 using the cyclic stress–strain curve, provided the isotropic parameters R_s and b have already been determined.

To determined R_s and b, we need experimental data which represent a relation between the cyclic stress range and the accumulated equivalent plastic strain. Such data should ideally be acquired through fully-reversed strain-controlled tests. In absence of such data, we used the data given in Figure 5 as a first approximation, which gives a relation between the stress range and the number of cycle. Integrating Eq. (16), we get

$$R = R_s(1 - e^{(-bp)}) \tag{28}$$

where the equivalent plastic strain can be approximated (by assuming that the plastic strain range is constant) as $p = N\Delta\varepsilon^p$, with $\Delta\varepsilon^p$ the plastic strain range in each cycle and N the number of cycles applied. Using this relation and assuming that the kinematic hardening is negligible, we arrive at the following equation between stress range and the number of cycles,

$$\frac{\Delta\sigma}{2} = \sigma_y + R_s(1 - e^{-bN\Delta\varepsilon^p}) \tag{29}$$

Fitting the above equation with the data given in Figure 5, we get $\frac{\sigma}{2} = 402 + 31.0(1 - e^{12.0p})$, which corresponds to $R_s = 31.0$ MPa and $b = 12.0$.

With R_s and b thus obtained, the constants k_1 and k_2 in Eq. (27) can then be determined from the cyclic stress-strain curve, such as the one shown in Figure 12 which presents the cyclic data from experiments conducted at McDonell Aircraft Company (MCAIR), together with some points obtained from the current study at steady state. For comparison, some data from the first cycle are also plotted. Evidently the cyclic stress-strain data are consistent among different sources, and as the data from MCAIR data covers a wider strain range it will be used to determine the material constants.

Figure 13 shows the result of a nonlinear curve-fitting using the model with a single back stress. The intersection at zero plastic strain range gives the yield stress as 307 MPa which also includes the contribution from the saturated isotropic hardening, and the material constants are determined as $k_1 = 73970.0$ and $k_2 = 560.0$. Evidently, the single back stress model can only accurately predict the stress-strain relationship when the strain range is small. In particular, it cannot correctly describe the continuing hardening feature when the strain exceeds 0.01, as shown in Figure 12, because the kinematic hardening term saturates at about $\Delta\varepsilon/2 = 0.006$, Figure 13, and the elastic strain is approximately 0.004.

To extend the applicable strain range, multiple back stresses can be introduced into the model, with each back stress evolving according to the same rule given in Eq. (6). Following similar derivation to that in Eq. (23 - 26), it can be proven that under uniaxial loading the relation between the cyclic stress and strain range can be given as

$$\frac{\Delta\sigma}{2} = \sum \frac{k_1^{(i)}}{k_2^{(i)}}\tanh\left(k_2^{(i)}\frac{\Delta\varepsilon^p}{2}\right) + R_s + \sigma_y, \tag{30}$$

where the material constants can be obtained from the same test data in a similar way as above. Figure 14 shows the curve fitting using the above model and the material constants are listed in Table 2.

In the following section, the above material models, both with a single back stress and multiple back stresses, will be used to simulate the mean stress relaxation under strain controlled cyclic loading.

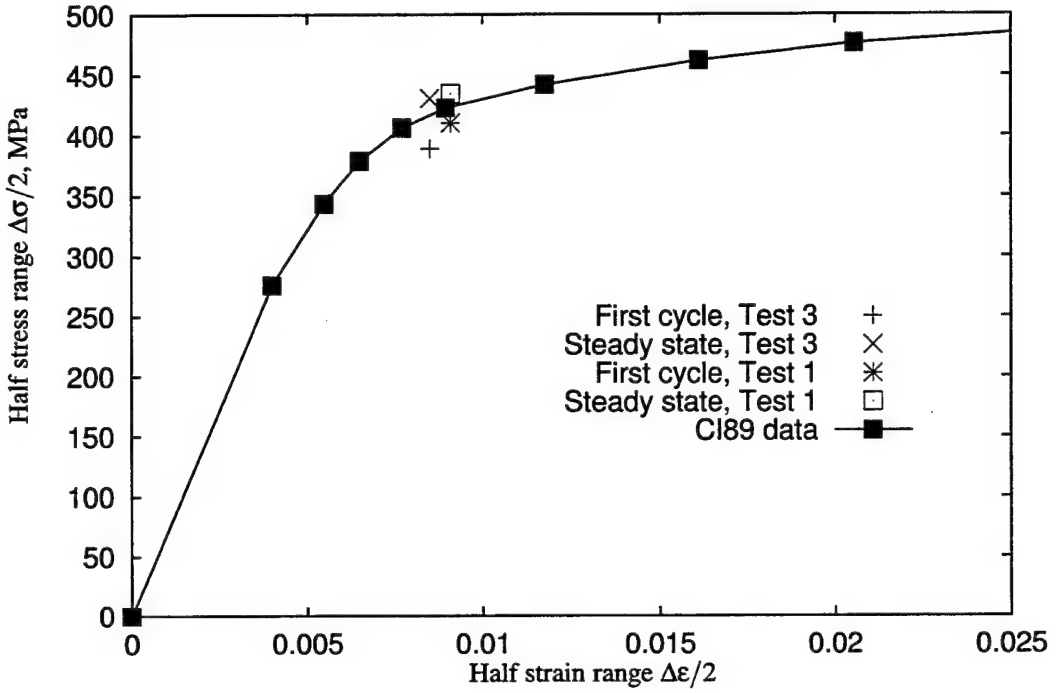

Figure 12: Cyclic stress-strain curve from various sources

4 Numerical Results

4.1 Single back stress model

Figure 15 presents the numerical results obtained from the model given in Section 3.3. For comparison, the experimental results for the first two cycles are also plotted. It can be seen from the figure that the model can well capture the general features of the hysteresis loops, such as the sign of the curvature and the general shape. A qualitative description of the progressive relaxation of the mean stress is also achieved, although the initial rate of relaxation is seen to be much higher than the experimental results. As mentioned earlier, for the single back stress model the kinematic hardening saturates quickly and beyond a certain strain the back stress assumes its maximum value of k_1/k_2. This effect, which is clearly demonstrated in the figure by the initial loading branch,

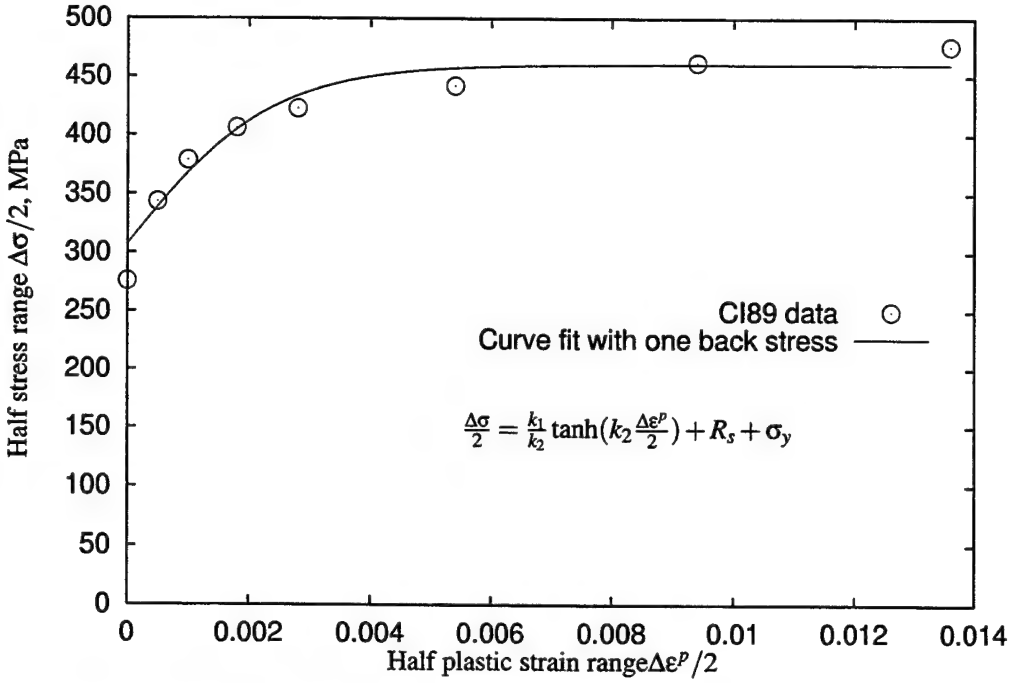

Figure 13: Material constants for kinematic hardening models with one back stress

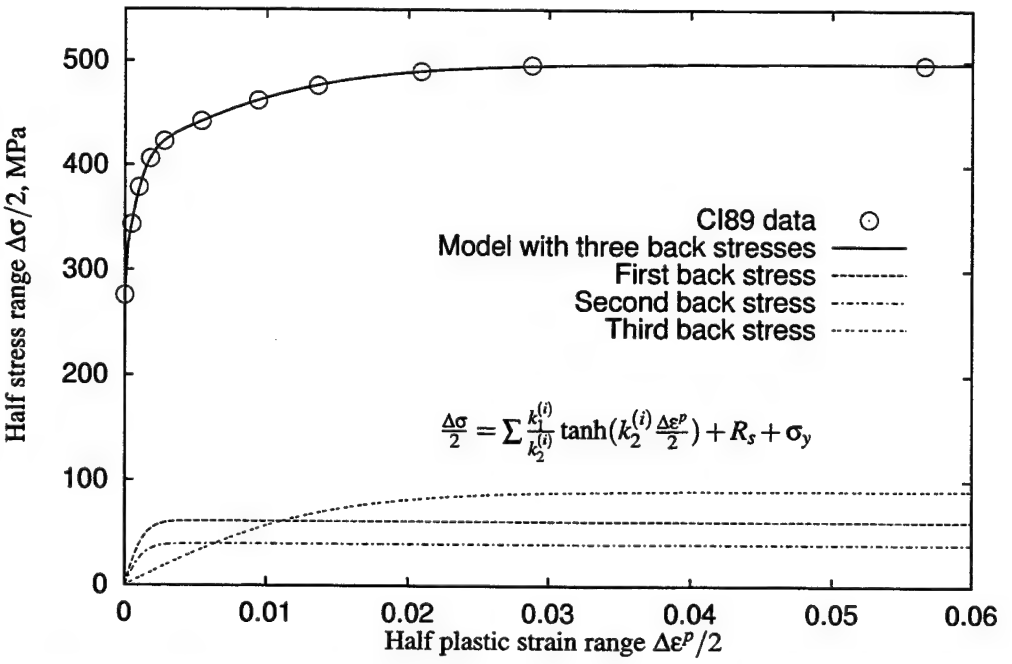

Figure 14: Material constants for kinematic hardening models with three back stresses

directly leads to the subsequent loops to shift downwards and contributes to the inaccuracies in the prediction of stress relaxation rate.

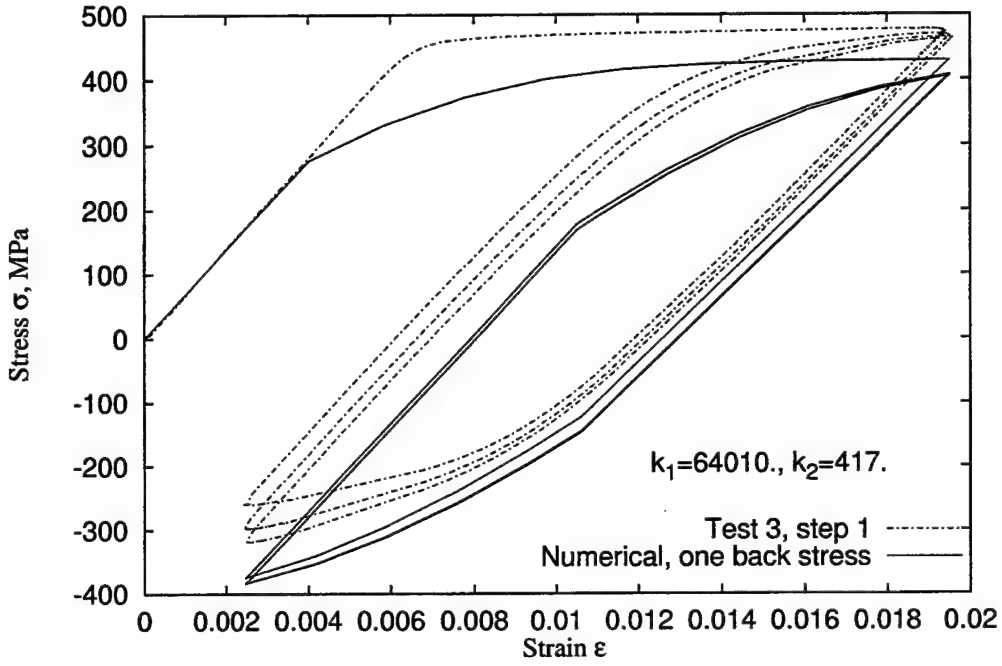

Figure 15: Numerical results for mean stress relaxation under strain-controlled cyclic loading

4.2 Multiple back stress model

It can be seen from Figure 15 that although the constitutive model presented in the previous section can capture the essential features of the cyclic loading such as the nonlinearity of the hysteresis loop and the progressive relaxation of the mean stress, it has two deficiencies, *i.e.*, it does not offer a smooth transition from elastic to plastic deformation, and it is only valid for small strain ranges. From Eq. (21) we can see that the slope of Z with respect to ε_p is given by

$$\frac{dZ}{d\varepsilon^p} = (k_1 - k_2 Z_0)e^{-\nu k_2(\varepsilon^p - \varepsilon_0^p)} \tag{31}$$

Therefore, the slope at elastic-plastic transition is proportional to k_1, which is generally smaller than the elastic modulus E, thus leading to an undesirable abrupt change of slope. In addition, the model with a single back stress has a limited strain range over which it is valid. Beyond this range the kinematic hardening will saturate to a constant value, as indicated in Eq. (21). To overcome this limitation, Chaboche (1986) suggested that multiple back stresses could be introduced, each evolves according to a similar rule as the one given in Eq. (6),

$$\dot{Z}_i = k_1^{(i)}\dot{\varepsilon}^p - k_2^{(i)} Z|\dot{\varepsilon}^p| \tag{32}$$

where $i = 1, \cdots, m$, and m is the number of back stresses. For proportional loading the above differential equation can still be integrated to get similar expressions as that given in Eq. (21),

$$Z_i = \nu \frac{k_1^{(i)}}{k_2^{(i)}} + \left(Z_{0i} - \nu \frac{k_1^{(i)}}{k_2^{(i)}} \right) \exp^{-\nu k_2^{(i)} (\varepsilon^p - \varepsilon_0^p)} \tag{33}$$

and the effective back stress is simple the sum of these components, *i.e.*, $Z = \sum Z_i$.

Figure 16 presents the numerical result obtained from a model with three back stresses, with the material constants listed in Table 2. Clearly, the model with multiple back stresses offers a smoother transition between the elastic and plastic deformation, and it improves the general shape of the hysteresis loop in comparison to the the experimental data.

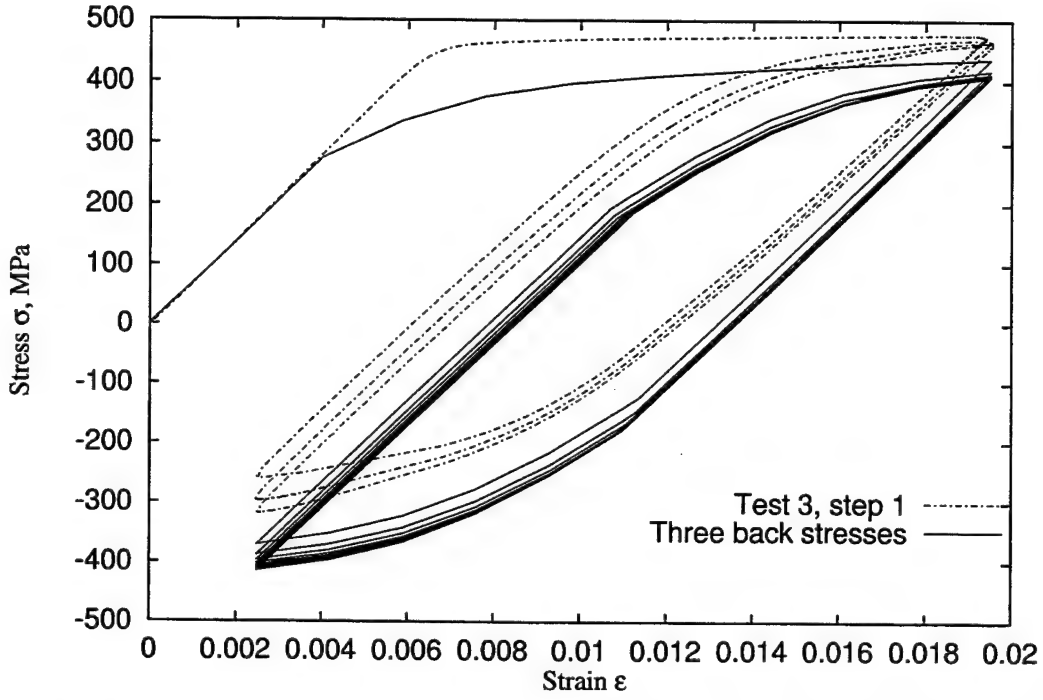

Figure 16: Numerical results for mean stress relaxation under strain -controlled cyclic loading. The parameters used are given in Table 2

k_1^1	63930.0	R_s	31.0
k_1^2	9980.0	b	12.0
k_1^3	6620.0		
k_2^1	734.0		
k_2^2	728.0		
k_2^3	73.0		

Table 2: Parameters for the constitutive model with multiple back stresses

4.3 Notch root stress

To use the above numerical model of cyclic plasticity to determine the fatigue life of components, it is necessary to consider the effect of stress concentration. In the following, a procedure for the determination of notch root stress and strain, based on Neuber's rule, is devised. Given the remote stress increment Δs and strain increment Δe, Neuber's rule states,

$$\Delta\sigma\Delta\varepsilon = K_t^2 \Delta s \Delta e \tag{34}$$

where K_t is the stress concentration factor, and $\Delta\sigma$ and $\Delta\varepsilon$ are the notch-root stress and strain increment, respectively. They are to be determined from Eq. (34) and the constitutive model. To derive a constitutive equation in total stress and strain, we denote $\Delta s = S - S_0$ and $\Delta e = e - e_0$, with S_0 and e_0 the remote stress and strain, respectively, at the previous turning point in the cyclic load history. Correspondingly, the local stress and strain increments are $\Delta\sigma = \sigma - \sigma_0$ and $\Delta\varepsilon = \varepsilon - \varepsilon_0$, respectively. Using these notations, the Neuber's rule can be rewritten as

$$(\varepsilon - \varepsilon_0)(\sigma - \sigma_0) = K_t^2 (s - s_0)(e - e_0). \tag{35}$$

Since the total stress is related to the total elastic strain through Hooke's law

$$\sigma = E(\varepsilon - \varepsilon^p), \tag{36}$$

we have

$$(\varepsilon - \varepsilon_0)(E\varepsilon - E\varepsilon^p - \sigma_0) = K_t^2 (s - s_0)(e - e_0), \tag{37}$$

which can be solved to give

$$\varepsilon = \frac{1}{2}\left(\varepsilon_0 + \varepsilon^p + \frac{\sigma_0}{E}\right) + \frac{1}{2}\nu\sqrt{\left(\varepsilon_0 + \varepsilon^p + \frac{\sigma_0}{E}\right)^2 - 4\left[\varepsilon_0\varepsilon^p + \frac{\sigma_0}{E}\varepsilon_0 - K_t^2(e - e_0)^2\right]}, \tag{38}$$

where $\nu = \pm 1$ depending on the direction of the plastic flow.

Using the above expression for ε in Eq. (36), the yield criterion can be expressed in terms of the current plastic strain ε^p,

$$\begin{aligned} f(\varepsilon^p) &= |\sigma(\varepsilon^p) - Z(\varepsilon^p)| - R(p) - \sigma_y \\ &= \nu[\sigma(\varepsilon^p) - Z(\varepsilon^p)] - R(p) - \sigma_y = 0, \end{aligned} \tag{39}$$

where the second equal sign is established by the fact that for the loading branch yielding can only occur when $\sigma > Z$, and for the unloading branch it can only occur when $Z > \sigma$. This nonlinear equation can be solved using the Newton method. When the plastic strain ε^p is determined, the strain can then be obtained from Eq. (38) and stress σ from Eq. (36).

Applying Newton's method to Eq. (39), we get

$$\varepsilon^p_{k+1} = \varepsilon^p_k - \frac{f(\varepsilon^p_k)}{\mathrm{d}f/\mathrm{d}\varepsilon^p} \tag{40}$$

where $\mathrm{d}f/\mathrm{d}\varepsilon^p$ is evaluated at $\varepsilon^p = \varepsilon^p_k$, and can be expressed as

$$\frac{\mathrm{d}f}{\mathrm{d}\varepsilon^p} = \nu\left(\frac{\mathrm{d}\sigma}{\mathrm{d}\varepsilon^p} - \frac{\mathrm{d}Z}{\mathrm{d}\varepsilon^p}\right) - \frac{\mathrm{d}R}{\mathrm{d}\varepsilon^p}. \tag{41}$$

and the expressions for $d\sigma/d\varepsilon^p$ and $dR/d\varepsilon^p$ can be derived explicitly as

$$\begin{aligned}\frac{d\sigma}{d\varepsilon^p} &= -\frac{E}{2}+\nu\frac{1}{2}\frac{\varepsilon^p+\sigma_0/E-3\varepsilon_0}{\sqrt{(\varepsilon_0+\varepsilon^p+\sigma_0/E)^2-4[\varepsilon_0\varepsilon^p+\sigma_0\varepsilon_0/E-K_t^2(e-e_0)^2]}}\\ \frac{dR}{d\varepsilon^p} &= \nu b R_0 e^{-bp}.\end{aligned} \tag{42}$$

where the relation $dp = \nu d\varepsilon^p$ has been used in the derivation of the second equation. The derivative $\frac{dz}{d\varepsilon^p}$ is given in Eq. (31) previously.

The algorithm for the above calculation is listed below

```
For each loading/unloading excursion Δe = e − e0
    Divide the remote strain range Δe into m parts
    For each remote strain ei
        Calculate yield function f
        If f > 0 then
loop:   Calculate df/dε^p and f
        Calculate d(ε^p) = −f/(df/d(ε^p)).
        Update:  ε^p_{k+1} = ε^p_k + d(ε^p).
        If |dε^p/ε^p_{k+1}| < 10^−6 exit.
        goto loop
        end if
    Calculate stress and strain using Eq. (38) and (36)
```

Figure 17 presents the notch root hysteresis loops obtained using the above algorithm. The stress concentration factor K_t is assumed to be 3.0, and the applied remote strain history has a minimum and maximum of -0.0001 and 0.004, respectively. This result clearly shows the feature of combined strain ratchetting and mean stress relaxation, consistent with the results reported by Wang and Rose (1998).

Assuming elastic-perfectly plasticity and prescribed stress limits, it is possible to derive an explicit relation between the ratchetting strain in each cycle and the material constants. For the model with a single back stress, Lemaitre and Chaboche (1990) has shown that

$$\delta\varepsilon^p = \frac{1}{k_2}\ln\left[\frac{(k_1/k_2)^2-(\sigma_{min}+\sigma_y)^2}{(k_1/k_2)^2-(\sigma_{max}-\sigma_y)^2}\right] \tag{43}$$

which shows that the maximum ratchetting is achieved when $\sigma_{min} = -\sigma_y$. When isotropic hardening is considered, such an explicit relation cannot be obtained.

4.4 Discussion

In the previous sections, the cyclic stress–strain behaviour of aluminium 7050 has been studied experimentally and numerically. It has been noted that under strain-controlled conditions, a

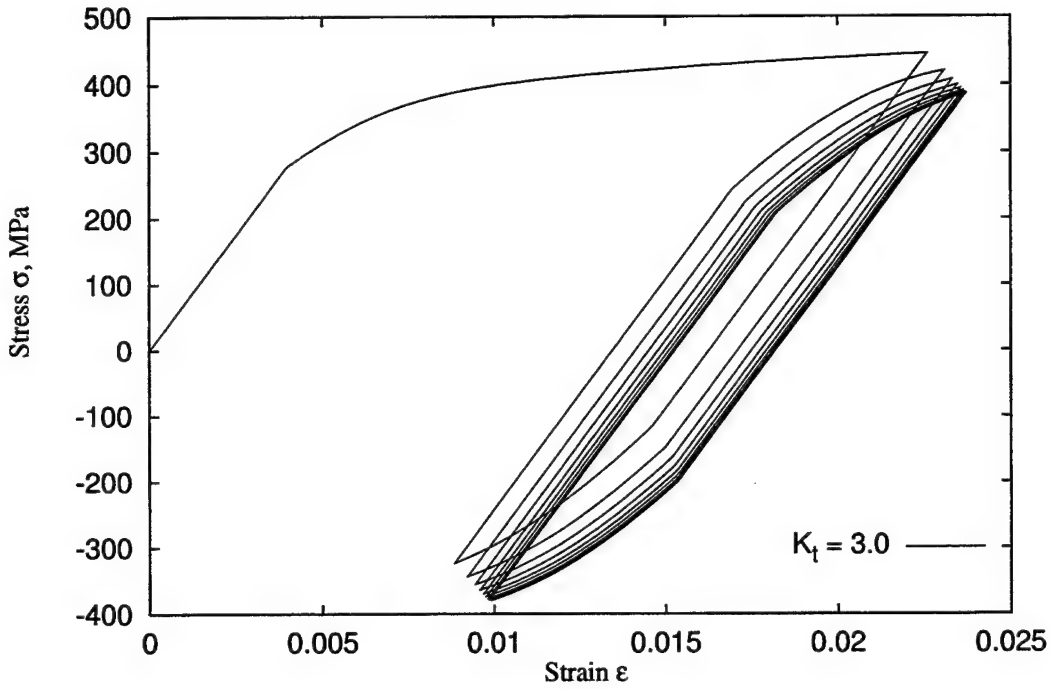

Figure 17: Numerical results for mean stress relaxation and strain ratchetting at notch root. The material constants are listed in 2.

nonzero mean stress will progressively approach zero, provided plastic deformation is induced in each cycle. By nature, this phenomenon is transient, as stable cycling can usually be achieved in a certain number of cycles. In this sense, its influence on the fatigue life of a component may be limited, especially for high cyclic fatigue. However, if the loading history includes occasional or periodic overloading, then taking into consideration of ratchetting would provide a more accurate description of the material stress–strain response.

Under stress-controlled condition, the situation is more complex. The strain ratchetting could be transient or continuous depending on the magnitude of the mean stress. Therefore, if the deformation is unconstrained structurally, and if there exists a high enough mean stress, the excessive plastic strain alone can lead to the failure of the component. This could be the case for components under combined torsional and tensile loading, such as the shaft of a helicopter

For most components the loading at critical locations, such as a notch root, is neither stress- nor strain-controlled. In this situation, the strain ratchetting will always be transient because the relaxation of the mean stress eventually eliminates the non-zero mean stress, which acts as the driving force for strain ratchetting. It should be pointed out that for critical locations with a low stress concentration, the effect of strain ratchetting would be more severe, if it exists at all, because in this case the plastic deformation is less constrained.

An ideal constitutive model should have the following characteristics: (a) be able to predict the shape of the hysteresis loops consistently; (b) be able to predict the rate of ratchetting/relaxation; (c) the material constants involved in the model should be few and can be determined easily. These seemingly simple requirements are actually hard to meet. For instance, while it is easy to reproduce the shape of one particular hysteresis loop by adjusting parameters, it is much more difficult to regenerate all the loops consistently. In the model discussed above, it has been noted that the ratchetting rate is too high for the first few cycles. This problem can be traced to the value of k_2 which represents the evanescence rate of the dynamic recovery that dictates the rate of ratchetting. One remedy is to introduce a threshold to k_2 to moderate the dynamic recovery (see Chaboche, 1991; Ohno, 1997, for example.). This will be addressed in future work.

5 Conclusions

The strain ratchetting behaviour of aluminium 7050 alloy has been studied experimentally and numerically. Under asymmetrical strain-controlled conditions test results demonstrate mean stress relaxation while asymmetrical strain-controlled tests show strain ratchetting, both characterised by the non-closure of hysteresis loops. While the mean stress progressively approaches zero, the strain ratchetting could continue at a constant rate for a sufficiently large mean stress and a non-zero plastic strain range.

The constitutive theory of nonlinear kinematic hardening has been investigated with a view to establishing a simple but effective model to represent the transient behaviour, to be incorporated into existing software such as `CI89`. A model with three back stresses has been established, which offers a reasonably accurate description of the cyclic behaviour. Using the existing experimental data, the material constants for the model have been determined, and the numerical results correlates well with the experimental ones.

A numerical procedure has also been devised for the calculation of the notch root stress and

strain using the current constitutive model. The numerical results show the expected feature of combined strain ratchetting and mean stress relaxation.

References

Armstrong, P. and Frederick, C. (1966). A mathematical representation of the multiaxial bauschinger effect. Technical report, CEGB Report: RD/B/N731, Berkeley Nuclear Laboratories.

Besseling, J. (1958). A theory of elastic, plastic and creep deformations of an initially isotropic material showing anisotropic strain hardening, creep recovoery and secondary creep. *ASME Journal of applied Mechanics*, 25:529–536.

Cernosky, E. and Krempl, E. (1980). A theory of viscoplasticity based on infinitesimal total strain. *Acta Mechanica*, 36:263–289.

Chaboche, J. (1991). On some modifications of kinematic hardening to improve the description of ratcheting effects. *International Journal of Plasticity*, 7.

Chaboche, J. and Nouailhas, D. (1989a). Constitutive modeling of ratchetting effects-part i: Experimental facts and properties of the classical models. *ASME Journal of engineering materials and technology*, 111:384–392.

Chaboche, J. and Nouailhas, D. (1989b). Constitutive modeling of ratchetting effects-part ii: Possibilities of some additional kinematic rules. *ASME Journal of engineering materials and technology*, 111:409–416.

Chaboche, J. L. (1986). Time-independent constitutive theories for cyclic plasticity. *International Journal of Plasticity*, 2(2):149–188.

Dafalias, Y. and Popov, E. (1976). Plastic internal variables formalism of cyclic plasticity. *ASME Journal of Applied Mechanics*, 43:645–651.

Glinka, G. (1985). Calculation of inelastic notch-tip strain–stress histories under cyclic loading. *Engineering Fracture Mechanics*, 22:839–854.

Inoue, T., Ohno, N., Suzuki, A., and Igari, T. (1989). Evaluation of inelastic constitutive models under plasticity-creep interaction for 2.1/4cr-1mo steel at 600degc. *Nuclear Engineering and Design*, 114:295–309.

Inoue, T., Yoshida, F., Ohno, N., Kawai, M., Niitsu, Y., and Imatani, S. (1991). Evaluationof inelastic constitutive models under plasticity-creep interaction in multiaxial stress state. *Nuclear Engineering and Desgin*, pages 1–11.

Jiang, Y. and Sehitoglu, H. (1996a). Modeling of cyclic ratchetting plasticity, part i: Development of constitutive relations. *Journal of Applied Mechanics, Transaction of the ASME*, pages 720–725.

Jiang, Y. and Sehitoglu, H. (1996b). Modeling of cyclic ratchetting plasticity, part ii: Comparison of model simulations with experiments. *Journal of Applied Mechanics, Transaction of the ASME*, pages 726–733.

Krieg, R. (1975). A practical two surface plasticity theory. *ASME Journal of Applied Mechanics*, 42:641–646.

Landgraf, R. W. (1970). The resistance of metals to cyclic deformation. In *Achievement of High Fatigue Resistance in Metals and Alloys*, pages 3–36. ASTP STP 467, AM. Soc. for Testing and Materials.

Lemaitre, J. and Chaboche, J. (1990). *Mechanics of Solid Materials*. Cambridge University Press.

Mroz, Z. (1967). On the description of anisotropic workhardening. *Journal of the Mechanics and Physics of Solids*, 15:163–175.

Neuber, H. (1961). Theory of stress concentration for shear-strained prismatical bodies with arbitrary nonlinear stress–strain law. *J. Applied Mechanics*, Vol. 26:544–550.

Ohno, N. (1997). Current state of the art in constitutive modelling for ratcheting. In *Trasaction of the 14th International Conference on Structural Mechanics in Reactor Technology*, Lyon, France.

Prager, W. (1949). Recent developments in the mathematical theory of plasticity. *Journal of Applied Physics*, 20:233–241.

Rousselier, G., Engel, J., and Masson, J. (1985). Etude comparative de models de comportement pour la simulation d'essais en traction-pression sur tubes en acier inoxydable. In *Document EDF-DER, annexe du Rapport no. 8 du GIS Rupture Ch̀aud.*

Stouffer, D. C. and Dame, L. T. (1996). *Inelastic Deformation of Metals*. John Wiley & Sons, Inc.

Wang, C. and Rose, L. (1998). Transient and steady-state deformation at notch rood under cyclic loading. *Mechanics of Materials*, pages 229 – 241.

Xia, Z. and Ellyin, F. (1991). Nonproportional multiaxial cyclic loading experiments and constitutive modelling. *ASME Journal of Applied Mechanics*, 58:317–325.

Xia, Z. and Ellyin, F. (1994). Biaxial ratcheting under strain of stress-controlled axial cycling with constant hoop stress. *Transaction of the ASME*, 61:422–428.

DISTRIBUTION LIST

Analysis of Cyclic Mean Stress Relaxation and Strain Ratchetting Behaviour of Aluminium 7050

W. Hu, C.H. Wang and S. Barter

	Number of Copies
DEFENCE ORGANISATION	
Task Sponsor	
DGTA	1
S&T Program	
Chief Defence Scientist FAS Science Policy AS Science Corporate Management	1
Director General Science Policy Development	1
Counsellor, Defence Science, London	Doc Data Sht
Counsellor, Defence Science, Washington	Doc Data Sht
Scientific Adviser Policy and Command	1
Navy Scientific Adviser	Doc Data Sht
Scientific Adviser, Army	Doc Data Sht
Air Force Scientific Adviser	1
Director Trials	1
Aeronautical and Maritime Research Laboratory	
Director, Aeronautical and Maritime Research Laboratory	1
Chief Airframes and Engine Division	1
Authors:	
W. Hu	5
C.H. Wang	1
S. Barter	1
L.F. Rose	1
L. Molent	1
D. Graham	1
K. Watters	1
DSTO Libraries	
Library Fishermens Bend	1
Library Maribyrnong	1
Library Salisbury	2
Australian Archives	1
Library, MOD, Pyrmont	Doc Data Sht

Capability Development Division

Director General Maritime Development	Doc Data Sht
Director General Land Development	Doc Data Sht
Director General C3I Development	Doc Data Sht

Army

ABCA Reports Distribution, Puckapunyal	4
SO (Science), DJFHQ(L), MILPO Enoggera, Queensland 4051	Doc Data Sht
NAPOC QWG Engineer NBCD c/- DENGRS-A, HQ Engineer Centre Liverpool Military Area, NSW 2174	Doc Data Sht
Establishment Library	1

Air Force

OIC ASI-LSA, DTA, HQLC	1

Intelligence Program

DGSTA Defence Intelligence Organisation	1

Corporater Support Program(libraries)

Officer in Charge, TRS, Defence Regional Library, Canberra	1
US Defense Technical Information Center	2
UK Defence Research Information Centre	2
Canada Defence Scientific Information Service	1
NZ Defence Information Centre	1

UNIVERSITIES AND COLLEGES

Australian Defence Force Academy Library Head of Aerospace and Mechanical Engineering	1
Deakin University, Serials Section (M List), Deakin University Library, Geelong, 3217	1
Senior Librarian, Hargrave Library, Monash University	1
Librarian, Flinders University	1
LaTrobe University Library	1
University of Melbourne, Engineering Library	1
Newcastle University, Library	1
University of Sydney, Engineering Library	1
UNSW, Physical Science Library	1
Queensland University, Library	1
Tasmania University, Engineering Library	1
University of Western Australia, Library	1

OTHER ORGANISATIONS

NASA (Canberra)	1

AGPS	1
OUTSIDE AUSTRALIA	
ABSTRACTING AND INFORMATION ORGANISATIONS	
INSPEC: Acquisitions Section Institution of Electrical Engineers	1
Library, Chemical Abstracts Reference Service	1
Engineering Societies Library, US	1
Materials Information, Cambridge Scientific Abstracts, US	1
Documents Librarian, The Centre for Research Libraries, US	1
SPARES	
	5
Total number of copies:	62

DEFENCE SCIENCE AND TECHNOLOGY ORGANISATION DOCUMENT CONTROL DATA				1. CAVEAT/PRIVACY MARKING
2. TITLE Analysis of Cyclic Mean Stress Relaxation and Strain Ratchetting Behaviour of Aluminium 7050			3. SECURITY CLASSIFICATION Document (U) Title (U) Abstract (U)	
4. AUTHOR(S) W. Hu, C.H. Wang and S. Barter			5. CORPORATE AUTHOR Aeronautical and Maritime Research Laboratory 506 Lorimer St, Fishermens Bend, Victoria, Australia 3207	
6a. DSTO NUMBER DSTO–RR–0153	6b. AR NUMBER AR 010–989	6c. TYPE OF REPORT Research	7. DOCUMENT DATE June 1999	
8. FILE NUMBER M1/9/616	9. TASK NUMBER AIR98/195	10. SPONSOR DGTA	11. No OF PAGES 28	12. No OF REFS 25
13. DOWNGRADING / DELIMITING INSTRUCTIONS Not Applicable			14. RELEASE AUTHORITY Chief, Airframes and Engines Division	

15. SECONDARY RELEASE STATEMENT OF THIS DOCUMENT

Approved For Public Release

OVERSEAS ENQUIRIES OUTSIDE STATED LIMITATIONS SHOULD BE REFERRED THROUGH DOCUMENT EXCHANGE CENTRE, DIS NETWORK OFFICE, DEPT OF DEFENCE, CAMPBELL PARK OFFICES, CANBERRA, ACT 2600

16. DELIBERATE ANNOUNCEMENT

No Limitations

17. CITATION IN OTHER DOCUMENTS

No Limitations

18. DEFTEST DESCRIPTORS

cyclic plasticity
strain ratchetting
aluminium 7050
constitutive modelling
mean stress relaxation
notch root stress

19. ABSTRACT

The cyclic constitutive behaviour of aluminium 7050 under elstoplastic deformation has been investigated in this report. Experiments were performed under strain-controlled and stress-controlled cyclic loading, respectively, with a view to quantify the phenomena of mean stress relaxation and strain ratchetting. To mathematically describe the experimentally observed cyclic stress-strain behaviour, the framework of constitutive theory for rate-independent plasticity has been reviewed and the state-of-art development in the field summarised. A detailed discussion has been presented for a class of constitutive models which uses nonlinear differential equations to describe the kinematic hardening, using a single back stress or multiple back stresses.

Using the available steady-state experimental data, the material constants in the model have been identified. A comparison to the experimental results shows that the model can provide very good representation of the material stress–strain behaviour under cyclic loading, in terms of the general shape of hysteresis loops. A numerical procedure for determining the notch-root stress and strain from the applied remote stress or strain has also been developed. The significance of strain ratchetting on the prediction of fatigue crack initiation and growth life has also been discussed.

Further study is needed to improve the accuracy of prediction in the rate of stress relaxation.